10-16-2017

# On the Dawn-Dusk Asymmetry of the Kelvin-Helmholtz Instability Between 2007 and 2013

Z. W. Henry
*Embry-Riddle Aeronautical University*, henryz@my.erau.edu

K. Nykyri
*Embry-Riddle Aeronautical University*, nykyrik@erau.edu

T. W. Moore
*Embry-Riddle Aeronautical University*, mooret14@my.erau.edu

A. P. Dimmock
*Aalto University*

X. Ma
*Embry-Riddle Aeronautical University*, max@erau.edu

AGU PUBLICATIONS

JGR

Journal of Geophysical Research: Space Physics

RESEARCH ARTICLE
10.1002/2017JA024548

# On the Dawn-Dusk Asymmetry of the Kelvin-Helmholtz Instability Between 2007 and 2013

Z. W. Henry[1], K. Nykyri[2], T. W. Moore[2], A. P. Dimmock[3], and X. Ma[2]

[1]Department of Aerospace Engineering, Embry-Riddle Aeronautical University, Daytona Beach, FL, USA, [2]Department of Physical Sciences, Embry-Riddle Aeronautical University, Daytona Beach, FL, USA, [3]Department of Electronics and Nanoengineering, Aalto University, Espoo, Finland

**Key Points:**
- Statistical study of the KHI occurrence rate shows a strong preference toward the dawnside for Parker-Spiral IMF
- A preference toward the duskside is observed for northward IMF
- The KH events are observed during higher SW speeds at the dusk sector

**Correspondence to:**
K. Nykyri,
nykyrik@erau.edu

**Citation:**
Henry, Z. W., Nykyri, K., Moore, T. W., Dimmock, A. P., & Ma, X. (2017). On the dawn-dusk asymmetry of the Kelvin-Helmholtz instability between 2007 and 2013. *Journal of Geophysical Research: Space Physics*, *122*. https://doi.org/10.1002/2017JA024548

Received 30 JUN 2017
Accepted 7 OCT 2017
Accepted article online 16 OCT 2017

**Abstract** Using data from Time History of Events and Macroscale Interactions during Substorms (THEMIS), a statistical study was performed to determine whether a dawn-dusk asymmetry exists in the occurrence rates of the Kelvin-Helmholtz instability during Parker-Spiral (PS) and Ortho-Parker-Spiral (OPS) orientations of the interplanetary magnetic field (IMF). It is determined from the data that there is a strong preference toward the dawnside during PS orientation, and although a preference to the duskside during OPS is suggested, this requires further study for an unambiguous confirmation. The uncertainty in the OPS result is due to a low number of events, which satisfied our selection criteria. Because IMF is statistically in PS orientation, the Kelvin-Helmholtz instability (KHI) preference for the dawn flank during this orientation may help explain the origin of the plasma sheet asymmetry of cold component ions because it has been shown that KHI can drive kinetic-scale wave activity capable of ion heating.

**Plain Language Summary** Velocity shear at the planetary boundary layers can form large-scale waves and vortices that can transport and heat plasma of solar wind origin into the magnetosphere. The present paper investigates dawn-dusk asymmetry of the observations of these Kelvin-Helmholtz (KH) waves during 6 years of Time History of Events and Macroscale Interactions during Substorms (THEMIS) spacecraft observations. The results clearly show a dawn-favored asymmetry of the KH occurrence rates. This may help explain the dawn-favored density and temperature asymmetry of the cold component ions of the Earth's magnetospheric plasma sheet, because KH waves have been linked to particle heating via secondary processes such as magnetic reconnection and kinetic wave activity.

## 1. Introduction

It has been well demonstrated that ions in the duskside plasma sheet are statistically hotter (see, e.g., Wang et al., 2012) than that in the dawn sector because the gradient and curvature drift affect more hot component ions, making them move more effectively to the dusk sector. However, the cold component ions are denser and hotter by ≈30–40% at the dawnside plasma sheet than those measured at the duskside (Hasegawa et al., 2003; Wing et al., 2005). A statistical study of magnetosheath temperatures using 7 years of Time History of Events and Macroscale Interactions during Substorms (THEMIS) data indicates that ion temperatures downstream of quasi-parallel (which is at the dawn flank for Parker-Spiral interplanetary magnetic field (IMF)) bow shock are only 15% higher than downstream of the quasi-perpendicular shock (Dimmock et al., 2015). This asymmetry that is likely related to foreshock processes or in situ magnetosheath physics is likely insubstantial to account for the magnitude of the plasma sheet temperature asymmetry. This suggests that asymmetric development of physical mechanisms at the magnetopause is responsible for this asymmetric heating and transport of cold component ions.

Ma and Otto (2014) showed that specific entropy increase (measure of nonadiabatic heating), during magnetic reconnection at the Earth's magnetopause is possible only if magnetosheath plasma beta is very low ($\beta \ll 1$). Because magnetosheath beta typically is of the order of unity, magnetic reconnection is likely not the sole process responsible for this heating.

Another key process at the magnetopause is Kelvin-Helmholtz instability (KHI), which is driven by the free energy of velocity shear. Because KHI can produce transport of mass, momentum, and energy across boundary

layers (Cowee et al., 2010; Ma et al., 2014a, 2017; Matsumoto & Hoshino, 2006; Miura, 1984; Nakamura et al., 2011; Nykyri & Otto, 2001, 2004; Otto & Fairfield, 2000; Thomas & Winske, 1993), it can play a significant role in magnetospheric dynamics. KHI can be stabilized by plasma compressibility and the magnetic tension force (Miura & Pritchett, 1982). The onset condition for the KH mode in an ideal, incompressible plasma with a discontinuous (arbitrarily thin) velocity shear layer is

$$\frac{m_0 n_1 n_2}{n_1 + n_2} \left[\mathbf{k} \cdot \Delta \mathbf{V}\right]^2 > \frac{1}{\mu_0} \left[\left(\mathbf{k} \cdot \mathbf{B}_1\right)^2 + \left(\mathbf{k} \cdot \mathbf{B}_2\right)^2\right], \tag{1}$$

where $m_0$ is the ion mass, $n$ is number density, $\Delta \mathbf{V} = \left(\mathbf{V}_1 - \mathbf{V}_2\right)$ is the velocity shear, $\mathbf{B}$ is magnetic field vector, $\mathbf{k}$ is KH wavevector, and the indices denote plasma properties on the two sides of the boundary (Chandrasekhar, 1961). Equation (1) suggested that magnetic field tangential to $\mathbf{k}$ vector of the KHI can resist deformation of the boundary. In contrast, when both velocity shear and magnetic shear exist in the the same plane and in same scale, velocity shear stabilizes the tearing mode, shutting it off when the flow is super-Alfvénic (Cassak, 2011; Cassak & Otto, 2011; Chen et al., 1997). Although plasma compressibility and a finite width of the shear flow can stabilize the KHI, Miura and Pritchett (1982 and Pu and Kivelson (1983) demonstrated that the influence for these is tiny for typical KH waves at the Earth's magnetopause. Because the events used for this study have been previously confirmed as KHIs (Kavosi & Raeder, 2015), the boundary condition for each one must be KH unstable.

Nykyri (2013) showed by using MHD simulations that KHI can grow more easily at the dawn flank magnetopause (with source region at the dawn-dusk terminator) during PS IMF orientation because the tangential magnetic field along the magnetopause is smaller at the dawnside (dawn-dusk terminator) than that at the duskside. The statistical observational study by Taylor et al. (2012) that found more KHI events at the dayside dusk flank magnetopause is not in contrast with this because in many of their events the horizontal IMF were not PS, but in OPS orientation, which would generate smaller tangential magnetic field along the duskside magnetopause for many of their events. On the other hand, the cold, dense plasmaspheric plume could also help excite KHI more easily at the dusk sector (Walsh et al., 2015).

While there exists dawn-dusk asymmetries in most of the magnetosheath plasma properties (Dimmock & Nykyri, 2013; Dimmock et al., 2014, 2015, 2016; Nykyri & Dimmock, 2016; Walsh et al., 2012, 2014), probably, the asymmetry of the IMF orientation has the strongest influence on the KHI development in each flank. Because IMF is statistically in PS orientation (see, for example, solar wind and IMF distributions in Dimmock and Nykyri, 2013), dawnside magnetospheric flank statistically has smaller tangential magnetic field. This could result in more KHI activity at the dawn sector and thus lead to more plasma heating at the dawnside flank associated with reconnection in KH vortices (Nishino et al., 2007; Nykyri et al., 2006) or heating via plasma waves associated with KHI (such as kinetic Alfvén waves created by mode conversion) (Johnson & Cheng, 2001; Johnson et al., 2001) or by kinetic magnetosonic waves (Moore et al., 2016).

The KH waves have been frequently observed at the magnetopause of Earth's low-latitude boundary layer during northward (Eriksson et al., 2016; Fairfield et al., 2000; Hasegawa et al., 2004; Lin et al., 2014), PS (Moore, 2012; Moore et al., 2016; Nykyri et al., 2006), southward IMF (Hwang et al., 2011; Yan et al., 2014), and also at the boundary layers of other planets (Boardsen et al., 2010; Delamere & Bagenal, 2010; Ma et al., 2015; Masters et al., 2010; McComas & Bagenal, 2008; Pope et al., 2009; Ruhunusiri et al., 2016; Sundberg et al., 2012).

A recent survey of in situ data from NASA's THEMIS mission between 2007 and 2013 has shown that Kelvin-Helmholtz (KH) waves are frequent at the magnetopause, occurring about 19% of the time during all magnetopause crossings (Kavosi & Raeder, 2015). This provides strong observational evidence as to their importance for magnetospheric dynamics. However, this study did not investigate the dawn-dusk asymmetry of the KHI. In the present paper we utilize the KHI event list published in Kavosi and Raeder (2015) and study the dawn-dusk asymmetry of the KHI and its dependence of the IMF PS versus OPS orientation. We also investigate the angle, $\theta$, between the $k$ vector of the KHI and velocity shear vector, $\mathbf{\Delta V}$, that maximizes the KHI onset condition.

The paper is organized as follows: the methodology is presented in section 2, the results are presented and discussed in section 3, and the conclusions are given in section 4.

**Table 1**
*Average Values for B (nT), V (kmİs), and $M_A$ in SW (Measured by OMNI) During KH Events Observed Under PS and OPS IMF on Either Flank*

| | $\|B\|_x$ | $\|B\|_y$ | $\|B\|_z$ | $B_t$ | $V_x$ | $V_y$ | $V_z$ | $M_A$ |
|---|---|---|---|---|---|---|---|---|
| Dawn PS | 3.49 | 3.45 | 1.46 | 5.64 | −390.1 | 3.36 | −2.77 | 9.99 |
| Dusk PS | 3.09 | 3.07 | 1.58 | 5.24 | −459.8 | −18.9 | −8.62 | 9.10 |
| Dawn OPS | 1.77 | 2.04 | 0.592 | 3.20 | −350.3 | −14.5 | 7.84 | 13.6 |
| Dusk OPS | 3.77 | 5.42 | 5.04 | 8.72 | −527.6 | 2.61 | −1.07 | 8.17 |

## 2. Methodology

### 2.1. Data and Instruments Used in the Study

The study utilizes data obtained from instruments on board the five THEMIS spacecraft (Angelopoulos, 2008). The fluxgate magnetometer instrument (Auster et al., 2008) on board each spacecraft provides full 3-D measurements of magnetic field. There are several time resolutions available which are FGS (3 s), FGL (0.25 s), and FGH (0.008 s). This study uses the FGS data. Plasma moments of velocity, density, pressure, and temperature are calculated on board by the electrostatic analyzer (ESA) instrument (McFadden et al., 2008) at a resolution of 3 s. The ESA instrument covers energy fluxes for ions between 5 eV to 25 keV and electrons from 6 eV to 30 keV. This study only uses ion moments of velocity and density. The upstream solar wind measurements are obtained from the virtual OMNI observatory (1 min resolution monthly data files are used) data base (King & Papitashvili, 2005). Note that the average of the total magnetic field value during each KH event, $B_t$, which is used to characterize certain KH event properties, is directly computed from $B_t$ array provided by OMNI. Therefore, the magnitude computed using the average values of $B_x$, $B_y$, and $B_z$ might differ from the average of the $B_t$ array (see Tables 1 and 2).

### 2.2. Upstream Binning Criteria

To categorize the IMF orientation as being PS, OPS, northward (NIMF), or southward (SIMF), the following conditions were imposed on the magnetic field given by the virtual OMNI in GSE coordinates, where $B_t$ is the total magnetic field magnitude: (1) Parker spiral if $B_x > 0.4B_t$ and $B_y < -0.4B_t$,*or* if $B_x < -0.4B_t$ and $B_y > 0.4B_t$; (2) Ortho-Parker spiral if $B_x > 0.4B_t$ and $B_y > 0.4B_t$,*or* if $B_x < -0.4B_t$ and $B_y < -0.4B_t$; (3) northward if $B_z > 0.5B_t$; and (4) southward if $B_z < -0.5B_t$

These conditions were checked for each THEMIS magnetopause crossing (MPC) whether it was a KH event or not, and any events that did not meet these conditions were removed from the data set. All remaining events were sorted according with respect to dawn/dusk position and to various conditions including IMF orientation, solar wind speed, and Alfvén mach number.

### 2.3. Time Lag and KH *k* Vector Orientation Calculation

The time ranges for both events and MPCs were taken from the list by Kavosi and Raeder (2015); THEMIS ephemeris and local **B** data were downloaded using SPEDAS version 1.00, and $\mathbf{V}_{SW}$, $\mathbf{B}_{SW}$, $\mathbf{B}_T$, and $M_A$ data were downloaded from the OMNIWeb data explorer. In order to account for the time lag between any OMNI measurements and the true time of the event, the time interval for upstream conditions was computed using the event interval and a time lag $\tau$, defined by equation (2). $\tau$ was computed for each event then subtracted from the limits of its respective THEMIS interval.

$$\tau = \frac{\Delta x}{V_{\mathrm{msh},x}}. \tag{2}$$

**Table 2**
*Average Values for B (nT), V (kmİs), and $M_A$ in SW (Measured by OMNI) During KH Events Observed Under NIMF and SIMF on Either Flank*

| | $B_x$ | $B_y$ | $B_z$ | $B_t$ | $V_x$ | $V_y$ | $V_z$ | $M_A$ |
|---|---|---|---|---|---|---|---|---|
| Dawn NIMF | 2.36 | −0.525 | 3.70 | 5.64 | −374.8 | 2.48 | 11.9 | 11.1 |
| Dusk NIMF | −0.147 | 0.247 | 3.95 | 5.43 | −533.9 | −13.5 | −0.0012 | 10.2 |
| Dawn SIMF | −0.0108 | 0.176 | −2.93 | 4.65 | −372.7 | 2.79 | −8.32 | 16.1 |
| Dusk SIMF | −0.435 | 1.04 | −3.77 | 5.85 | −450.6 | −1.87 | −13.4 | 9.22 |

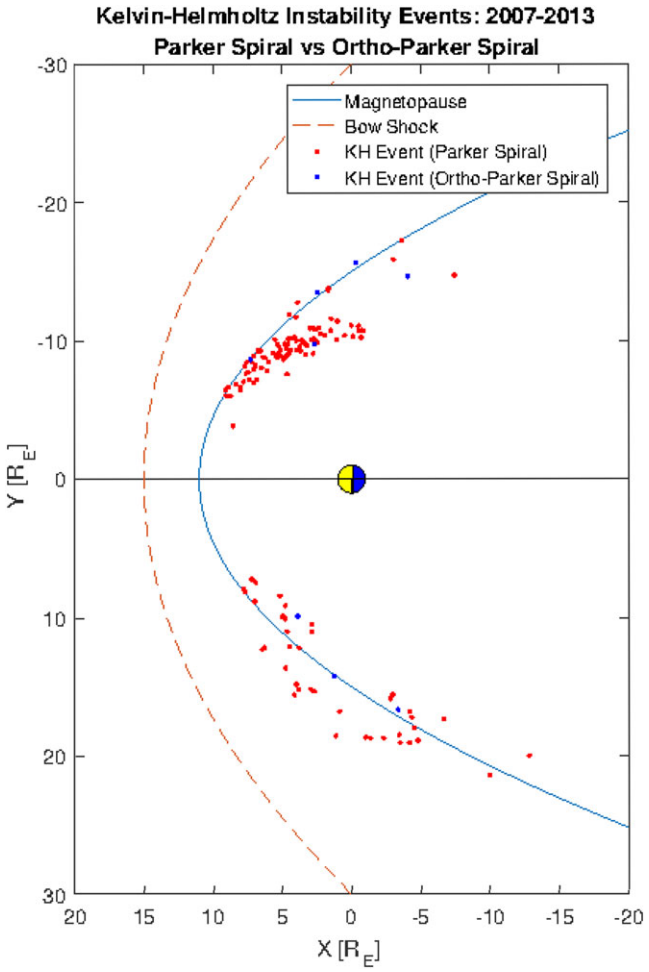


**Figure 1.** Kelvin-Helmholtz instability event locations, divided into Parker Spiral and Ortho-Parker Spiral. The magnetopause and bow shock lines are parabolic approximations for the purpose of orientation.

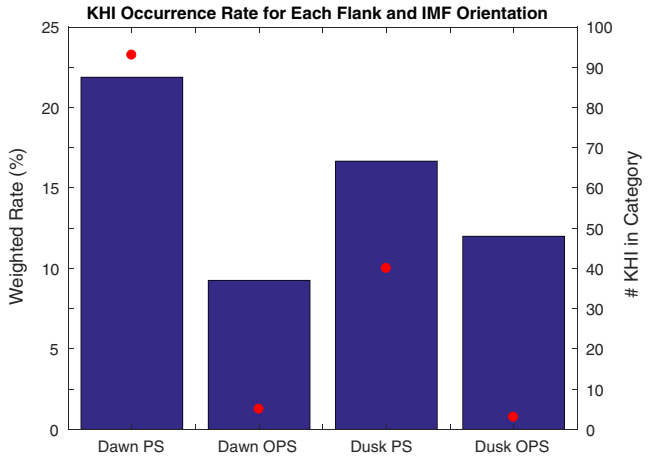


**Figure 2.** Weighted dawn-dusk KHI occurrence rates during PS and OPS. Bars represent the percent of all MPCs during corresponding IMF orientation which were KH, and the circles represent the absolute number of events listed in each category.

Here $\Delta x$ is the $x$ distance from the relevant THEMIS spacecraft to the bow shock nose and $V_{msh,x}$ is the average magnetosheath speed in the $x$ direction over the duration of the event. In order to determine whether the THEMIS data interval was in the magnetosheath (MSH) or in the magnetospheric (MSP)-like plasma region, $\frac{n}{T}$ was computed for all data points in each event, where $n$ and $T$ are the ion density and temperature, respectively. The largest 25% of these data were averaged with the lowest 25% of the data, and this value was taken to be $\frac{n}{T}$ at the magnetopause. The points for **B**, **V**, and $n$ that corresponded to $\frac{n}{T} < \frac{n_{msp}}{T_{msp}}$ were assigned to the MSP side, and those that corresponded to $\frac{n}{T} > \frac{n_{msp}}{T_{msp}}$ were assigned to the MSH side. The first 33% of the data for each KH event in magnetosheath (MSH) and magnetospheric (MSP) side of the boundary were used to compute the average $\mathbf{B}_{msp}$, $\mathbf{B}_{msh}$, $\Delta\mathbf{V} = \mathbf{V}_{msh} - \mathbf{V}_{msp}$, $n_{msp}$, and $n_{msh}$. Equation (1) was reorganized as

$$\frac{\mu_0 m_0 n_{msh} n_{msp}}{n_{msh} + n_{msp}} \frac{(\mathbf{k} \cdot \Delta\mathbf{V})^2}{(\mathbf{B}_{msh} \cdot \mathbf{k})^2 + (\mathbf{B}_{msp} \cdot \mathbf{k})^2} > 1 \tag{3}$$

and was then used to determine which angle, $\theta$ , between **k** vector and **ΔV** maximized the onset criteria, assuming the average boundary normal was perpendicular to the [**ΔV**, **k**] plane.

## 3. Results and Discussion

With the aforementioned filters applied to the 406 listed KH events, 33% were determined to occur during PS orientation, 2% during OPS orientation, 15% were NIMF, and 14% were SIMF. The locations of the PS and OPS events may be seen in Figure 1. This scatterplot serves as a visualization of the data distribution over the entire set.

### 3.1. Normalization of Occurrence Rates on Dawn and Dusk Flanks

At a first glance, far more events are observed on the dawn flank, and the majority of the events occur during PS orientation. Using THEMIS orbital phase data, we determined that most of the MPCs listed occurred on the dawn flank. Therefore, the occurrences of KHIs for any given upstream solar wind (SW) condition were weighted with respect to amount of MPCs during the corresponding SW conditions. The result of this may be seen in Figure 2. Each bar represents the weighted occurrence rate of the KH on dawn and dusk flanks by the percentage of MPCs on either flank during both orientations which were KH, while the red circles indicate the total number of KH events in each category. This data summary shows a clear preference of KH toward the dawn flank during PS, and weighted occurrence rates suggests that duskside has more events during OPS than to dawn sector. However, statistically the dusk KH preference for OPS orientation is insignificant because there are only few events for OPS IMF orientation. Indeed, the duskside still has more events during PS than during OPS. This is likely because IMF is more seldom in OPS orientation than in PS orientation. Similarly, Figure 3 displays weighted occurrences of KHIs in either NIMF or SIMF. There is a strong preference to the duskside during NIMF and a slight preference during SIMF.

Tables 1 and 2 show the average of the mean IMF components, SW velocity, and SW Alfvén Mach number during each KH event categorized according to prevailing IMF orientation. It is clear from Tables 1 and 2 that the dusk flank KH events occur during higher SW velocity and during lower Alfvén Mach number than the events at the dawn flank.

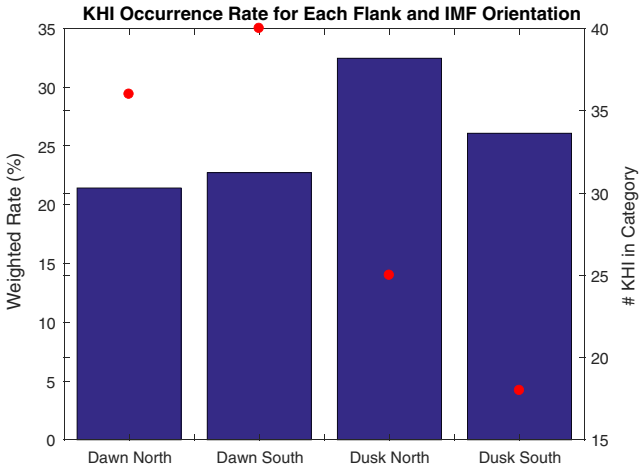


**Figure 3.** Weighted KHI dawn versus dusk occurrence rates for NIMF and SIMF. Note that the lower *y* limit for the raw # of KHI events is 15.

### 3.2. Normalization of Occurrence Rates in Angular Segments

To more deeply explore the summary shown in these figures, the KHIs were split into eight angular sectors based on angle between THEMIS probe and *x* coordinate, where negative angles, $\alpha$, represent the dawnside and positive angles indicate the duskside. Regions are divided into 30° increments from dayside up to ±90°, and final region is 60° wide extending to ±150°.

Figure 4 shows the occurrence rate distribution in two separate bar graphs: one for PS and one for OPS. Most KH occur at the dawn sector between −60° to −90° during PS orientation and the normalized occurrence rates during OPS are highest at dusk sector between 60 to 90°. The dawn preference during PS is still evident in this figure; however, the OPS becomes more ambiguous due to the low number of data points. The same type of information is shown for NIMF and SIMF in Figure 5. Normalized occurrence rates indicate that KHI favors dusk sector during NIMF, while most events during SIMF occur at dawn sector between −60° and −90°.

### 3.3. Angular KH Occurrence Rate Dependence on Alfvén Mach Number and $V_{SW}$

Figure 6 shows the normalized occurrence rate of all observed KH events at different angular sectors during different Alfvén Mach number ranges: $M_A < 5; 5 < M_A < 10; 10 < M_A < 15; 15 < M_A < 20; M_A > 25$. Most KH events (≈78) occur at the dawn sector between $\alpha = -60$ and −90° for $5 < M_A < 10$and for the low solar wind Mach numbers ($M_A < 5$), the largest normalized KH occurrence rates are at the dusk sector for $\alpha = -30$ to −60°. For the very high Mach number ($M_A > 20$), all KH events occur at the dawn sector.

High values of $M_A$ suggest either a high velocity or a low Alfvén speed, which depends on magnetic field and plasma density. Figure 7 shows the occurrence rates in the same angular segments while separating the events by $V_{SW}$. There is a preference to the dawnside when $V_{SW}$ is relatively low (<450 km/s), and this asymmetry shifts to the duskside when $V_{SW} > 450$ km/s.

A statistical study using 5 years of THEMIS data in the magnetosheath and comparison to MHD simulations by Dimmock and Nykyri (2013) shows that the magnetosheath downstream of quasi-perpendicular shock (typically the dusk sector) has higher magnetic field strength than the dawn sector, while the densities showed very little asymmetry. On the other hand, a slight dawn favored density asymmetry has been reported close to the magnetopause during THEMIS mission (Dimmock et al., 2016; Walsh et al., 2012), but this asymmetry is not so clear in the central magnetosheath (Dimmock & Nykyri, 2013; Dimmock et al., 2016). The lower densities and higher magnetic field strengths close to magnetopause at the dusk flank would result in higher Alfvén speed than on the dawn flank. This could explain why KH events observed in the dusk sector typically occur for higher solar wind speeds than at the dawn sector and that there are events at dusk for strongly PS orientation, because increased velocity shear will help overcome the magnetic tension.

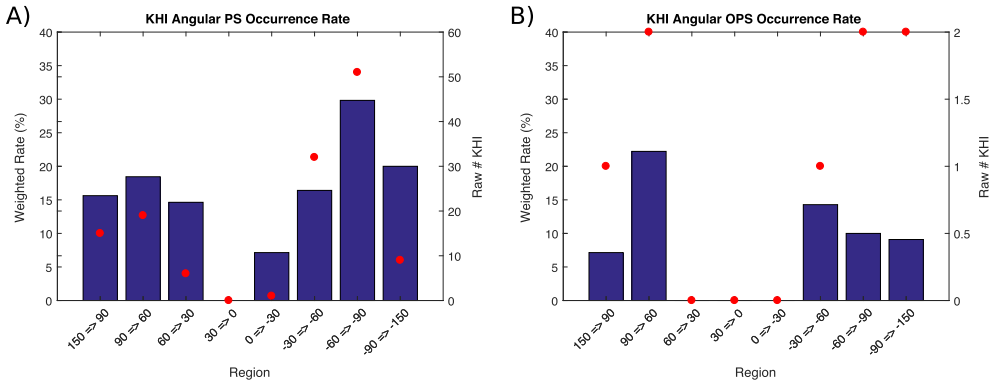


**Figure 4.** Weighted occurrence rates of KHI during PS and OPS, separated into angle segments. Positive angles indicate the duskside, whereas negative angles indicate the dawnside. The 0° marks noon on the dayside.

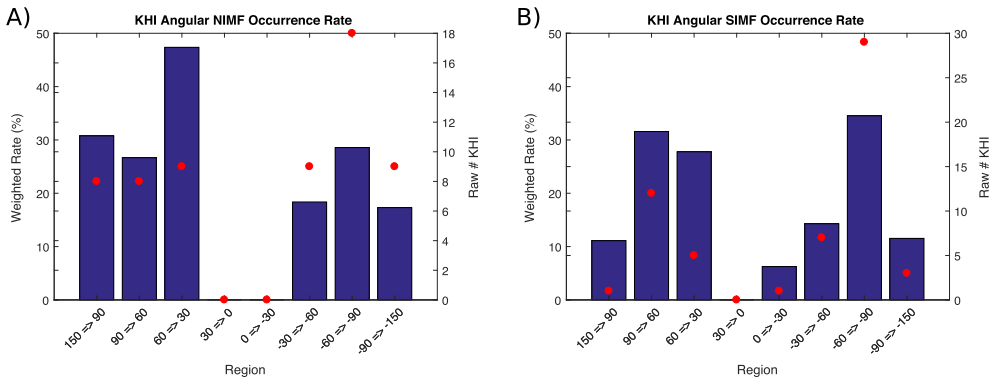


**Figure 5.** Weighted occurrence rates of KHI during NIMF and SIMF, separated into angular segments.

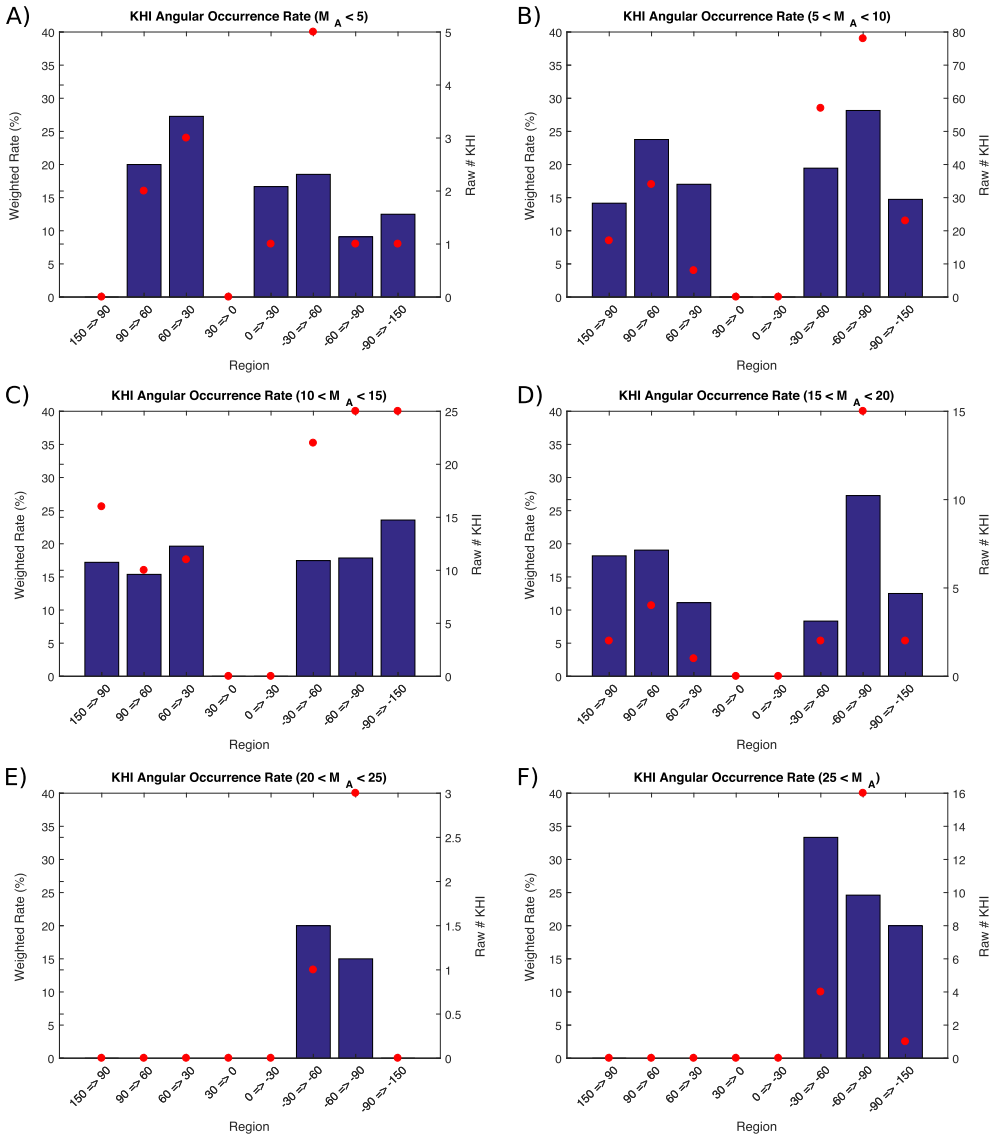


**Figure 6.** Weighted occurrence rates of KHI for varying Alfvén Mach numbers, separated into angular segments.

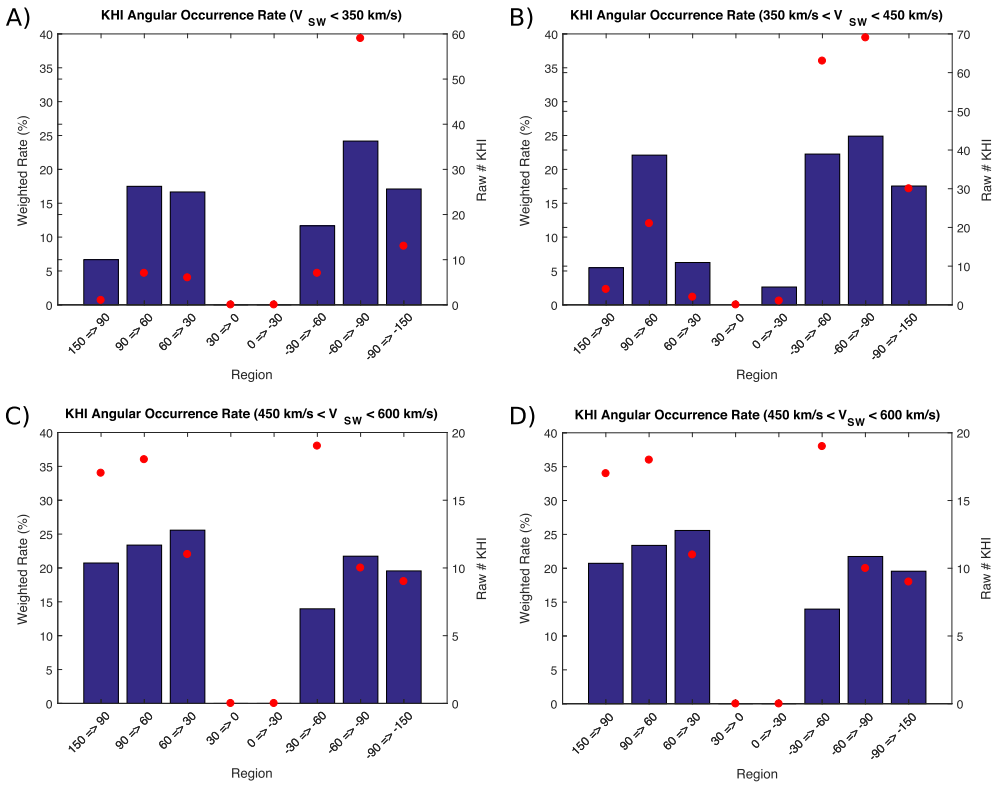


**Figure 7.** Weighted occurrence rates of KHI for different solar wind velocity ranges.

### 3.4. Propagation Angle of KHI for Maximizing the KH Onset Condition

Adamson et al. (2016) and Nykyri et al. (2006) demonstrated using Cluster data and 2-D and 3-D MHD simulations that the **k** vector of the KHI does not need to be aligned with maximum velocity shear but that KH waves can propagate with an angle from the equatorial plane to minimize the tangential magnetic field tension to maximize the onset criteria. Cluster data during the KH event and 2-D MHD simulations were consistent with the propagation angle of 35° (Nykyri et al., 2006), whereas the 3-D investigation of the angle maximizing the onset criteria was 48° and corresponding angle observed in 3-D MHD simulation was 41° (Adamson et al., 2016). To explore this statistically for the present set of KH events, equation (3) was applied in order to determine the propagation angle with respect to the shear flow velocity that maximized the onset criteria for each event. The distribution of the angles for maximizing the left side of the inequality is shown in Figure 8. For majority of the events the KH onset criteria are maximized for $-32° < \theta < 12°$. This plot also reveals some events with very high propagation angles. It is clear that the KHI cannot propagate perpendicular to shear flow plane. We therefore checked the THEMIS data for all the events for which our algorithm obtained $|\theta| > 60°$ and which were listed as KHI in Kavosi and Raeder (2015). Five of these events (see the appendix for further information) do not seem to have characteristics of the KHI and had "propagation" angles of −73.5°, 73.6°, −60.7°, −87.1°, and 60.2°, respectively.

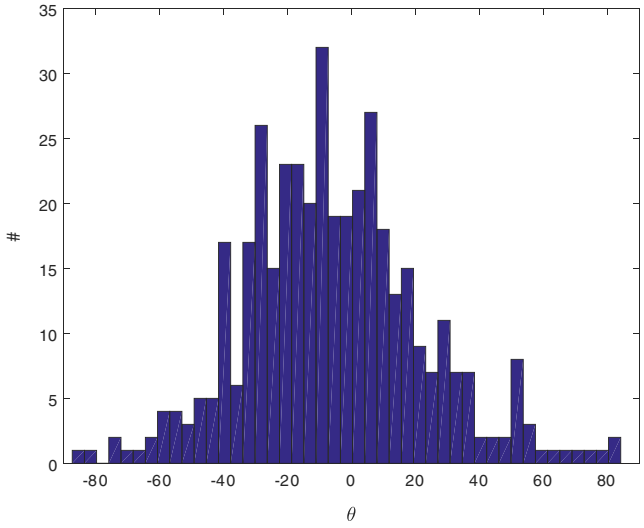


**Figure 8.** Number distribution (#) of the $\theta$ angles of the KH events with respect to the velocity shear vector for maximizing the KH onset condition.

Figure 9 shows the average angle between KH **k** vector and the velocity shear vector, $\Delta\mathbf{V}$, that maximizes the onset criteria for each KH event categorized based on the orientation of the IMF, at dawn (blue) and dusk (red) flanks, respectively. The average SW speed during each category is denoted by white columns. It is evident that for PS, OPS, and SIMF orientations of the IMF, the average magnitude of the $\theta$ angles is slightly larger ($23° < |\theta| < 26°$) at the dawn sector than that at the dusk ($21° < |\theta| < 23°$). During NIMF the $\theta$ angles are nearly the same (difference only within 1° smaller at dusk) at both flanks,

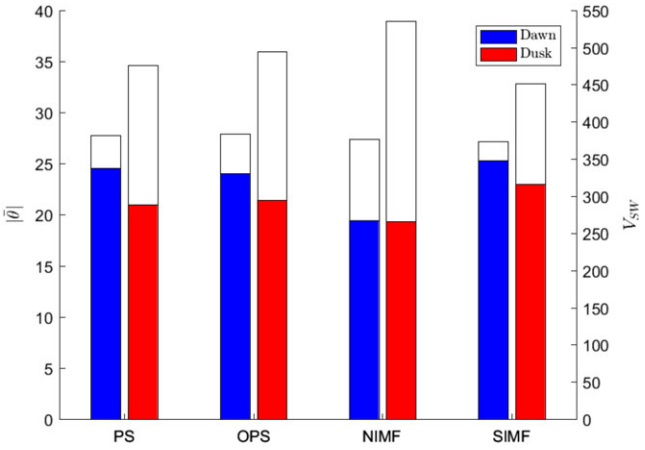


**Figure 9.** Average magnitudes of **k** vector angles in degrees with respect to velocity shear vector that maximizes the onset criteria for KH events categorized based on the orientation of the IMF, at dawn (blue) and dusk (red) flanks, respectively. The average prevailing SW speed in km/s is indicated by white column with scale on the right side of the *y* axis.

which is to be expected based on symmetry argument. However, it is very clear that the KH events during NIMF at dusk occur during much higher SW speed ($V_{SW} \approx 530$ km/s) than at dawn ($V_{SW} \approx 380$ km/s).

Based on IMF draping geometry during PS IMF, it would be expected that dusk flank has a stronger tangential magnetic field (Nykyri, 2013), so that average $\theta$ would be larger at dusk flank during PS than that at dawn. However, the SW speed for dusk KH events during PS orientation is higher ($V_{SW} \approx 480$ km/s) than for dawn flank events ($V_{SW} \approx 380$ km/s), which will make it possible for KH to propagate with smaller angle with respect to shear flow plane in order to maximize the onset criteria. For the OPS IMF orientation one would expect higher average magnitude of the $\theta$ angle at the dawn sector than at dusk, which indeed is indicated in these graphs. However, we like to remind the reader that there are not enough events for the OPS orientation to make definite conclusion at this time.

For SIMF, the average $\theta$ angles at the dawn sector are larger by few degrees than the dusk sector, which is interesting considering that for the NIMF orientation the situation is more symmetric. When solely considering the KH onset criteria, the purely SIMF and NIMF orientations for the same plasma parameters will give the same KH growth. However, this is more true for prolonged periods of NIMF or SIMF. If the interval is short, the IMF properties before and after the interval of interest can play a role. Also, in a real system the IMF is never perfect NIMF or SIMF but always has some finite spiral angle, so some bias can be introduced from this. Our IMF selection criteria ensured that $B_z$ is dominant, but $B_x$ and $B_y$ might still be a couple of nanoteslas. To address the effect of this horizontal IMF in $x, y$ plane for our event statistics at the dawn and dusk flanks during NIMF and SIMF intervals, respectively, we have further analyzed these events. Figure 10 shows $B_z$ normalized to $B_T$ versus the IMF angle ($\tan^{-1}(B_x/B_y)$) in $x, y$ plane from the $x$ axis. Perfect PS (OPS) corresponds to −45° (+45° ). The red (blue) dots indicate when KH event was classified occurring during NIMF (SIMF), black triangles (circles) indicate events during PS and OPS IMF, and black dots indicate when none of the above binning criteria were satisfied. Red (blue) triangles indicate when event was classified both as PS and NIMF (SIMF), and red (blue) circles indicate when event was classified both as OPS and NIMF (SIMF). The statistics detailing the overlap is as follows: At the dawn flank 16.67% of the KH events occurring during NIMF are also categorized as PS and 2.78% as OPS, while 12.5% of SIMF events are also PS and 0% are OPS. At the dusk flank 4% of the KH events occurring during NIMF are also categorized as PS and 4% as OPS, while 33.3% of SIMF events are also PS and 11.11% are OPS. Except for KH events (33.33%) at the dusk magnetopause that are both classified as SIMF and PS, the overlap for other conditions is rather small (<17%). Table 3 shows the average solar wind speed and Alfvén Mach number for each of the four overlapping categories (presented as blue or red triangles and circles in Figure 10) in each flank, indicating that at the dusk the KHIs are observed for very high solar wind speeds

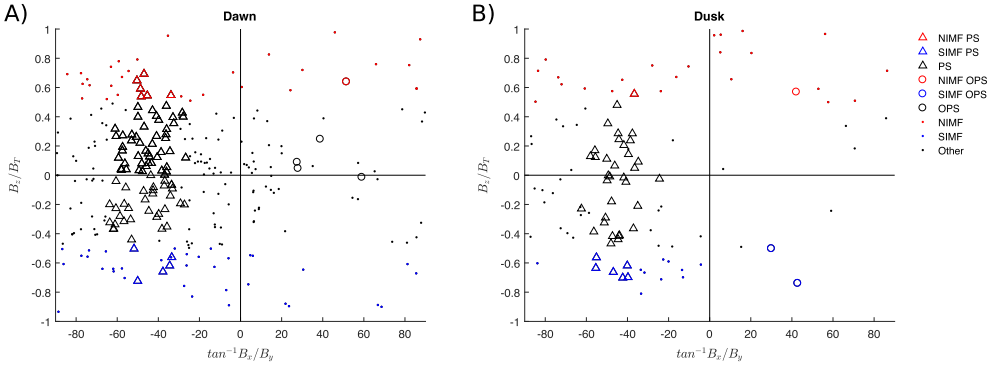


**Figure 10.** Average $\frac{B_z}{B_T}$ versus average IMF angle ($\tan^{-1}(B_x/B_y)$) in $x, y$ plane from the $x$ axis for each KH event at dawn and dusk flanks, respectively. The −45° (+45° ) corresponds to the pure PS (OPS) IMF orientation, respectively. Note that the KH intervals with average $\frac{B_z}{B_T} > 0.5\ B_T$ are classified as NIMF and the intervals with average $\frac{B_z}{B_T} < -0.5\ B_T$ as SIMF in Figures 3, 5, and 9.

**Table 3**
*Average Solar Wind Speed (km/s) and Alfvén Mach Number for All Events in Each Quadrant of Figure 10*

| | North PS | North OPS | South PS | South OPS |
|---|---|---|---|---|
| Dawn $\|V\|$ | 397.3 | 355.0 | 390.3 | 374.8 |
| Dusk $\|V\|$ | 523.8 | 518.0 | 468.8 | 443.9 |
| Dawn $M_A$ | 10.5 | 16.2 | 10.9 | 16.9 |
| Dusk $M_A$ | 9.95 | 9.91 | 9.65 | 8.82 |

for NIMF when the horizontal IMF is in PS orientation. This makes sense, as overcoming the magnetic tension more velocity shear is required. At dusk, the KH events also occur for higher solar wind speeds for NIMF than for SIMF, probably because during NIMF the boundary layer is thicker due to flux pile up at the dayside, while for SIMF the dayside reconnection can create a thinner boundary. Another interesting feature that initially seems counterintuitive based on the reduced magnetic tension argument is that at the dawn flank the NIMF cases that are also classified as PS occur during slightly higher SW speeds than the OPS cases. This is probably because the solar wind $M_A$ is much higher for OPS cases (16–17) than for PS cases (10–11) at the dawn sector, indicating that the strength of the IMF is slightly higher at dawn for events which were classified both as NIMF or SIMF and PS.

The growth rate of MHD KH instability is mostly determined by the the direction of the magnetic field, which is well summarized by equation (1) (Chandrasekhar, 1961). It is well known that compressibility can reduce the KH growth rate (Miura & Pritchett, 1982; Pu & Kivelson, 1983). However, Pu and Kivelson (1983) pointed out that for typical conditions occurring on the Earth's magnetopause the effect from compressibility is very tiny (e.g., section 5 in Pu & Kivelson, 1983). Furthermore, a typical KH wavelength at the Earth's magnetopause (i.e., 2–6 Earth's radii (Otto & Fairfield, 2000) is about 10 to 50 times longer than the the typical width of magnetosheath-magnetospheric boundary (Dunlop et al., 2001). For such a long KH wavelength, Miura and Pritchett (1982) demonstrated that both compressibility and finite initial sheared flow width have minor effect on the KH growth rate (see Figures 3 and 4 in Miura & Pritchett, 1982). Therefore, we think that using equation (1) is sufficient for the purpose of this study.

Furthermore, when considering the 3-D dynamics and the real magnetospheric topology, during SIMF magnetic reconnection can also operate at the vicinity of the dayside magnetopause, which can result in complicated magnetic field geometries, especially when KHI is also operating. Ultimately, the interaction of KHI and reconnection in 3-D depends on which of these starts as a primary mechanism (Ma et al., 2014a, 2014b).

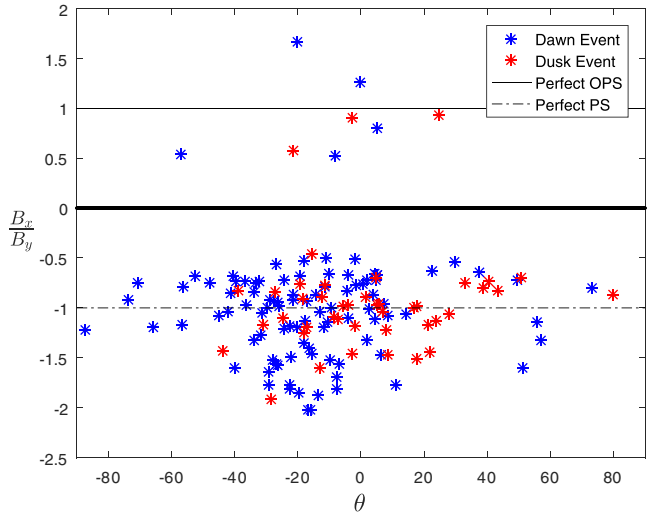


**Figure 11.** $\frac{B_x}{B_y}$ versus $\theta$ of **k** vector with respect to the velocity shear vector. Perfectly PS and OPS IMF orientations occur at −1 and 1, respectively.

Figure 11 shows a scatter plot of $\frac{B_x}{B_y}$ versus $\theta$ for dawn (blue) and dusk (red) KH events. The majority of KHI events are centralized near $\pm 1$ but are offset slightly. The trimmed averages for OPS and PS $\frac{B_x}{B_y}$ are 0.8985 and $-1.075$, respectively, indicating that a typical KH event is likely to occur when $|B_x| \approx |B_y|$. Like discussed before, it is also evident from this graph that most KH events occur at the dawn sector for PS orientation with $\theta \approx -20^\circ$.

## 4. Conclusions and Discussion

In the present paper we have studied the dawn-dusk asymmetry of the KHI between 2007 and 2013 using THEMIS data and its occurrence dependence in relation to four prevailing IMF orientations: northward IMF (NIMF), southward IMF (SIMF), Parker Spiral (PS) IMF and Ortho-Parker-Spiral (OPS) IMF, solar wind speed, and the Alfvén Mach number. The main conclusions are as follows:

1. There is an overall preference to the dawnside for KHIs.
2. The KH events are observed at the dusk sector for higher SW speeds.
3. During PS IMF, there is a significant preference to the dawn flank of the magnetopause.
4. A preference to dusk is suggested for OPS, but more data will need to be collected before proper conclusions may be drawn.
5. The weighted occurrence rates of the KHI show preference for the dusk during NIMF.
6. Average magnitude of the angle, $|\theta|$, between KH **k** vector and velocity shear vector is larger at the dawn sector for all IMF conditions than that at the dusk sector.

These results that show dawn flank preference of the KHI during PS orientation strongly support the idea that dawn-favored asymmetry of the density and temperature of the cold component plasma sheet ions is driven by asymmetric development of the KHI. Both reconnection in KH vortices (Nishino et al., 2007; Nykyri et al., 2006) and ion-scale wave generation by the KHI (Johnson & Cheng, 2001; Johnson et al., 2001; Moore & Nykyri, 2017; Moore et al., 2016) has been linked to ion heating. Furthermore, while Ma and Otto (2014) showed that significant heating due magnetic reconnection is possible only for very low magnetosheath plasma beta, it may be possible that compression of the magnetic field by the KHI can generate low beta regions, so that shocks associated with 3-D reconnection in KH vortices may provide effective heating. This effect may be further enhanced for low solar wind Alfvén Mach numbers. We will return to this topic in our future work.

An interesting result is that KH events at the dusk flank are observed during much higher SW speeds than those at the dawn sector. Considering that for the same SW conditions and PS orientation the dusk flank has higher velocities than the dawn (Dimmock & Nykyri, 2013), this could be partly explained because spacecraft happens to be at the flank with typically higher speeds (dusk).

The other aspect is that the NIMF and SIMF orientations still have some horizontal IMF, so when on average the horizontal component of IMF is predominantly in PS orientation, there is more magnetic tension on average on the dusk sector (even for NIMF or SIMF), so KH would not be observed at the dusk sector unless the SW and resulting magnetosheath speed was somewhat higher. Figures 1 and 4 indeed suggest that there are slightly more tailward events ($X < -2\,R_E$ and $90^\circ \leq \alpha \leq 150^\circ$) at the dusk sector for PS orientation, where the strong tangential magnetic field can be overcome by higher velocity shear.

Finally, we note that in order to draw definite conclusions that KHI operates more readily at the dusk flanks during OPS, more data at the dusk flanks need to be collected. Ideally, it would be beneficial to study KH simultaneously at dawn and dusk flanks for range of solar wind conditions, which will likely be possible during future Magnetosphere Multi-Scale and THEMIS orbital phases.

## Appendix A: Magnetic Field and Plasma Parameters

All the Kelvin-Helmholtz events for which our analysis gave propagation angles greater than 60° were checked. Figure A1 shows magnetic field and plasma parameters for five of these events with very high propagation angles, which do not seem to have typical characteristics of the KHI. We do not think that these are KH events.

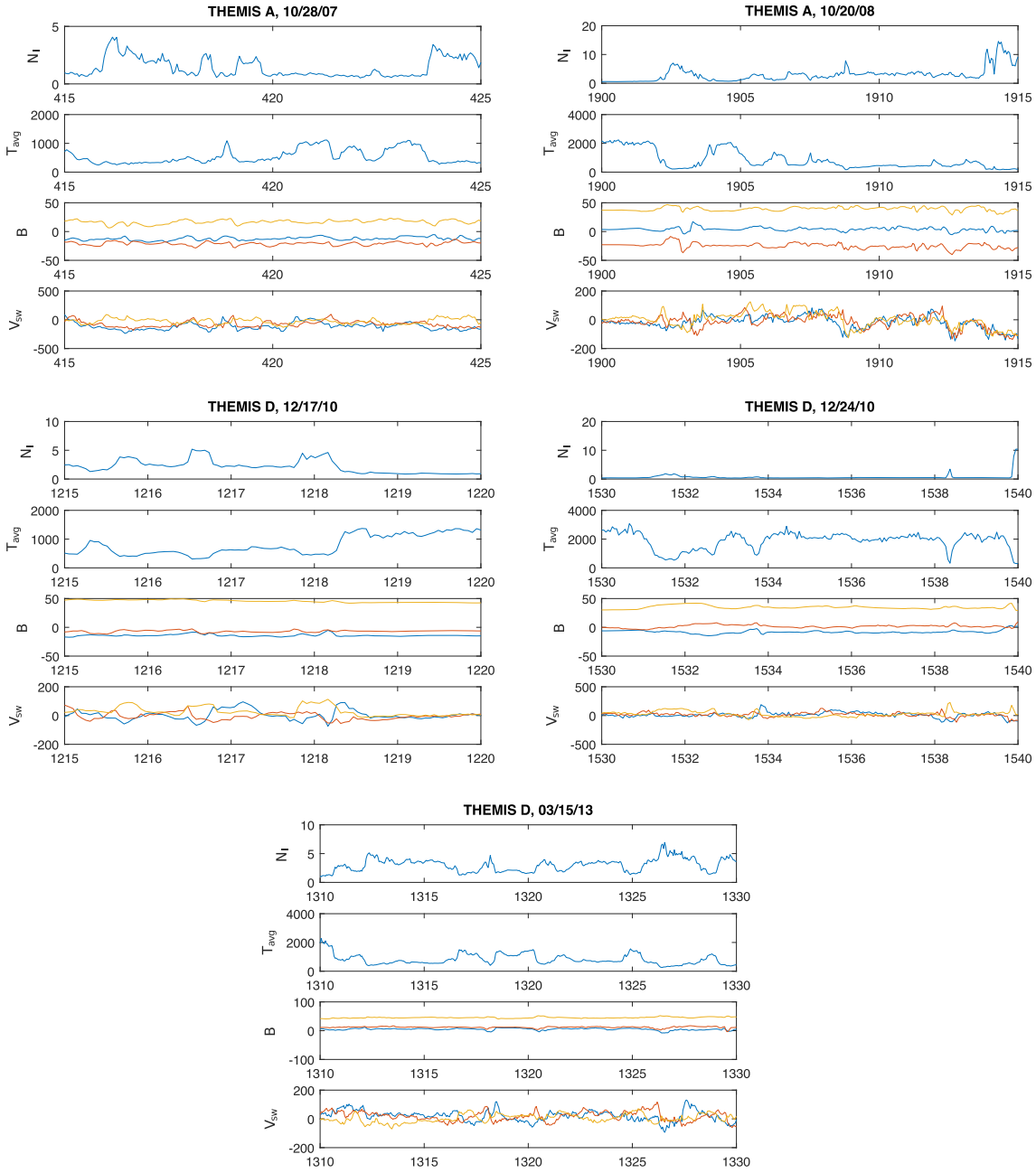


**Figure A1.** Five events listed as KHI in Kavosi and Raeder (2015), for which our algorithm obtained highly oblique $\theta$ angles. These may not be KH events.

**Acknowledgments**
The work of Z. H., K. N., and T. M. was supported by NSF GEM grant 1502774, and work of KN and XM was also supported by NASA grant NNX16AF89G. The work of A. D. was supported by the Academy of Finland grant 288476. The authors would also like to thank Kavosi and Raeder for providing the times for KH events and magnetopause crossings (Kavosi & Raeder, 2015). We acknowledge use of NASA/GSFC Space physics Data Facility OMNIWeb (http://omniweb.gsfc.nasa.gov) service,

## References

Adamson, E., Nykyri, K., & Otto, A. (2016). The Kelvin-Helmholtz instability under Parker-Spiral interplanetary magnetic field conditions at the magnetospheric flanks. *Advances in Space Research*, *58*, 218–230. https://doi.org/10.1016/j.asr.2015.09.013

Angelopoulos, V. (2008). The THEMIS mission. *Space Science Reviews*, *141*, 5–34. https://doi.org/10.1007/s11214-008-9336-1

Auster, H. U., Glassmeier, K. H., Magnes, W., Aydogar, O., Baumjohann, W., Constantinescu, D., … Wiedemann, M. (2008). The THEMIS fluxgate magnetometer. *Space Science Reviews*, *141*, 235–264. https://doi.org/10.1007/s11214-008-9365-9

Boardsen, S. A., Sundberg, T., Slavin, J. A., Anderson, B. J., Korth, H., Solomon, S. C., & Blomberg, L. G. (2010). Observations of Kelvin-Helmholtz waves along the dusk-side boundary of Mercury's magnetosphere during MESSENGER's third flyby. *Geophysical Research Letters*, *37*, L12101. https://doi.org/10.1029/2010GL043606

Cassak, P. A. (2011). Theory and simulations of the scaling of magnetic reconnection with symmetric shear flow. *Physics of Plasmas*, *18*(7), 072106. https://doi.org/10.1063/1.3602859

Cassak, P. A., & Otto, A. (2011). Scaling of the magnetic reconnection rate with symmetric shear flow. *Physics of Plasmas*, *18*(7), 074501. https://doi.org/10.1063/1.3609771

Chandrasekhar, S. (1961). *Hydrodynamic and hydromagnetic stability*. New York: Oxford University Press.

and OMNI data. Authors would also like to thank the THEMIS instrument teams for the use of their data.

Chen, Q., Otto, A., & Lee, L. C. (1997). Tearing instability, Kelvin-Helmholtz instability, and magnetic reconnection. *Journal of Geophysical Research*, *102*, 151–161.

Cowee, M. M., Winske, D., & Gary, S. P. (2010). Hybrid simulations of plasma transport by Kelvin-Helmholtz instability at the magnetopause: Density variations and magnetic shear. *Journal of Geophysical Research*, *115*, A06214. https://doi.org/10.1029/2009JA015011

Delamere, P. A., & Bagenal, F. (2010). Solar wind interaction with Jupiter's magnetosphere. *Journal of Geophysical Research*, *115*, A10201. https://doi.org/10.1029/2010JA015347

Dimmock, A. P., & Nykyri, K. (2013). The statistical mapping of magnetosheath plasma properties based on THEMIS measurements in the magnetosheath interplanetary medium reference frame. *Journal of Geophysical Research: Space Physics*, *118*, 4963–4976. https://doi.org/10.1002/jgra.50465

Dimmock, A. P., Nykyri, K., & Pulkkinen, T. I. (2014). A statistical study of magnetic field fluctuations in the dayside magnetosheath and their dependence on upstream solar wind conditions. *Journal of Geophysical Research: Space Physics*, *119*, 6231–6248. https://doi.org/10.1002/2014JA020009

Dimmock, A. P., Nykyri, K., Karimabadi, H., Osmane, A., & Pulkkinen, T. I. (2015). A statistical study into the spatial distribution and dawn-dusk asymmetry of dayside magnetosheath ion temperatures as a function of upstream solar wind conditions. *Journal of Geophysical Research: Space Physics*, *120*, 2767–2782. https://doi.org/10.1002/2014JA020734

Dimmock, A. P., Pulkkinen, T. I., Osmane, A., & Nykyri, K. (2016). The dawn-dusk asymmetry of ion density in the dayside magnetosheath and its annual variability measured by THEMIS. *Annales Geophysicae*, *34*(5), 511–528. https://doi.org/10.5194/angeo-34-511-2016

Dunlop, M. W., Balogh, A., Cargill, P., Elphic, R. C., Fornaçon, K.-H., Georgescu, E., … FGM team (2001). Cluster observes the Earth's magnetopause: Coordinated four-point magnetic field measurements. *Annales Geophysicae*, *19*(10/12), 1449–1460. https://doi.org/10.5194/angeo-19-1449-2001

Eriksson, S., Lavraud, B., Wilder, F. D., Stawarz, J. E., Giles, B. L., Burch, J. L., … Goodrich, K. A. (2016). Magnetospheric multiscale observations of magnetic reconnection associated with Kelvin-Helmholtz waves. *Geophysical Research Letters*, *43*, 5606–5615. https://doi.org/10.1002/2016GL068783

Fairfield, D. H., Otto, A., Mukai, T., Kokubun, S., Lepping, R. P., Steinberg, J. T., … Yamamoto, T. (2000). Geotail observations of the Kelvin-Helmholtz instability at the equatorial magnetotail boundary for parallel northward fields. *Journal of Geophysical Research*, *105*, 21,159–21,174.

Hasegawa, H., Fujimoto, M., Maezawa, K., Saito, Y., & Mukai, T. (2003). Geotail observations of the dayside outer boundary region: Interplanetary magnetic field control and dawn-dusk asymmetry. *Journal of Geophysical Research*, *108*(A4), 1163. https://doi.org/10.1029/2002JA009667

Hasegawa, H., Fujimoto, M., Phan, T.-D., Reme, H., Balogh, A., Dunlop, M. W., … TanDokoro, R. (2004). Transport of solar wind into Earth's magnetosphere through rolled-up Kelvin-Helmholtz vortices. *Nature*, *430*, 755–758.

Hwang, K.-J., Kuznetsova, M. M., Sahraoui, F., Goldstein, M. L., Lee, E., & Parks, G. K. (2011). Kelvin-Helmholtz waves under southward interplanetary magnetic field. *Journal of Geophysical Research*, *116*, A08210. https://doi.org/10.1029/2011JA016596

Johnson, J. R., & Cheng, C. Z. (2001). Stochastic ion heating at the magnetopause due to kinetic Alfvén waves. *Geophysical Research Letters*, *28*, 4421–4424.

Johnson, J. R., Cheng, C. Z., & Song, P. (2001). Signatures of mode conversion and kinetic Alfvén waves at the magnetopause. *Geophysical Research Letters*, *28*, 227–230.

Kavosi, S., & Raeder, J. (2015). Ubiquity of Kelvin-Helmholtz waves at Earth's magnetopause. *Nature Communications*, *6*, 7019. https://doi.org/10.1038/ncomms8019

King, J. H., & Papitashvili, N. E. (2005). Solar wind spatial scales in and comparisons of hourly Wind and ACE plasma and magnetic field data. *Journal of Geophysical Research*, *110*, A02104. https://doi.org/10.1029/2004JA010649

Lin, D., Wang, C., Li, W., Tang, B., Guo, X., & Peng, Z. (2014). Properties of Kelvin-Helmholtz waves at the magnetopause under northward interplanetary magnetic field: Statistical study. *Journal of Geophysical Research: Space Physics*, *119*, 7485–7494. https://doi.org/10.1002/2014JA020379

Ma, X., & Otto, A. (2014). Nonadiabatic heating in magnetic reconnection. *Journal of Geophysical Research: Space Physics*, *119*, 5575–5588. https://doi.org/10.1002/2014JA019856

Ma, X., Otto, A., & Delamere, P. A. (2014a). Interaction of magnetic reconnection and Kelvin-Helmholtz modes for large magnetic shear: 1. Kelvin-Helmholtz trigger. *Journal of Geophysical Research: Space Physics*, *119*, 781–797. https://doi.org/10.1002/2013JA019224

Ma, X., Otto, A., & Delamere, P. A. (2014b). Interaction of magnetic reconnection and Kelvin-Helmholtz modes for large magnetic shear: 2. Reconnection trigger. *Journal of Geophysical Research: Space Physics*, *119*, 808–820. https://doi.org/10.1002/2013JA019225

Ma, X., Stauffer, B., Delamere, P. A., & Otto, A. (2015). Asymmetric Kelvin-Helmholtz propagation at Saturn's dayside magnetopause. *Journal of Geophysical Research: Space Physics*, *120*, 1867–1875. https://doi.org/10.1002/2014JA020746

Ma, X., Delamere, P., Otto, A., & Burkholder, B. (2017). Plasma transport driven by the three-dimensional Kelvin-Helmholtz instability. *Journal of Geophysical Research: Atmospheres*, *122*. https://doi.org/10.1002/2017JA024394

Masters, A., Achilleos, N., Kivelson, M. G., Sergis, N., Dougherty, M. K., Thomsen, M. F., … Coates, A. J. (2010). Cassini observations of a Kelvin-Helmholtz vortex in Saturn's outer magnetosphere. *Journal of Geophysical Research*, *115*, A07225. https://doi.org/10.1029/2010JA015351

Matsumoto, Y., & Hoshino, M. (2006). Turbulent mixing and transport of collisionless plasmas across a stratified velocity shear layer. *Journal of Geophysical Research*, *111*, A05213. https://doi.org/10.1029/2004JA010988

McComas, D. J., & Bagenal, F. (2008). Reply to comment by S. W. H. Cowley et al. on "Jupiter: A fundamentally different magnetospheric interaction with the solar wind". *Geophysical Research Letters*, *35*, L10103. https://doi.org/10.1029/2008GL034351

McFadden, J. P., Carlson, C. W., Larson, D., Ludlam, M., Abiad, R., & Elliott, B. (2008). The THEMIS ESA plasma instrument and in-flight calibration. *Space Science Reviews*, *141*, 277–302. https://doi.org/10.1007/s11214-008-9440-2

Miura, A. (1984). Anomalous transport by magnetohydrodynamic Kelvin-Helmholtz instabilities in the solar wind magnetosphere interaction. *Journal of Geophysical Research*, *89*, 801–818. https://doi.org/10.1029/JA089iA02p00801

Miura, A., & Pritchett, P. L. (1982). Nonlocal stability analysis of the MHD Kelvin-Helmholtz instability in a compressible plasma. *Journal of Geophysical Research*, *87*, 7431–7444. https://doi.org/10.1029/JA087iA09p07431

Moore, T. (2012). Identifying signatures of plasma waves and reconnection associated with Kelvin-Helmholtz activity (MS thesis). Daytona Beach, FL: Embry-Riddle Aeronautical University.

Moore, T. W., Nykyri, K., & Dimmock, A. P. (2017). Ion-scale wave properties and enhanced ion heating across the low-latitude boundary layer during Kelvin-Helmholtz instability. *Journal of Geophysical Research: Space Physics 122*. https://doi.org/0.1002/2017JA024591

Moore, T. W., Nykyri, K., & Dimmock, A. P. (2016). Cross-scale energy transport in space plasmas. *Nature Physics*, *12*, 1164–1169. https://doi.org/10.1038/NPHYS3869

Nakamura, T. K. M., Hasegawa, H., Shinohara, I., & Fujimoto, M. (2011). Evolution of an MHD-scale Kelvin-Helmholtz vortex accompanied by magnetic reconnection: Two-dimensional particle simulations. *Journal of Geophysical Research*, *116*, A03227. https://doi.org/10.1029/2010JA016046

Nishino, M. N., Fujimoto, M., Ueno, G., Mukai, T., & Saito, Y. (2007). Origin of temperature anisotropies in the cold plasma sheet: Geotail observations around the Kelvin-Helmholtz vortices. *Annales Geophysicae*, *25*, 2069–2086.

Nykyri, K. (2013). Impact of MHD shock physics on magnetosheath asymmetry and Kelvin-Helmholtz instability. *Journal of Geophysical Research: Space Physics*, *118*, 5068–5081. https://doi.org/10.1002/jgra.50499

Nykyri, K., & Dimmock, A. P. (2016). Statistical study of the ULF Pc4-Pc5 range fluctuations in the vicinity of Earth's magnetopause and correlation with the low latitude boundary layer thickness. *Advances in Space Research*, *58*, 257–267. https://doi.org/10.1016/j.asr.2015.12.046

Nykyri, K., & Otto, A. (2001). Plasma transport at the magnetospheric boundary due to reconnection in Kelvin-Helmholtz vortices. *Geophysical Research Letters*, *28*, 3565–3568. https://doi.org/10.1029/2001GL013239

Nykyri, K., & Otto, A. (2004). Influence of the Hall term on KH instability and reconnection inside KH vortices. *Annales Geophysicae*, *22*, 935–949. https://doi.org/10.5194/angeo-22-935-2004

Nykyri, K., Otto, A., Lavraud, B., Mouikis, C., Kistler, L., Balogh, A., & Réme, H. (2006). Cluster observations of reconnection due to the Kelvin-Helmholtz instability at the dawn side magnetospheric flank. *Annales Geophysicae*, *24*, 2619–2643.

Otto, A., & Fairfield, D. H. (2000). Kelvin-Helmholtz instability at the magnetotail boundary: MHD simulation and comparison with Geotail observations. *Journal of Geophysical Research*, *105*, 21,175–21,190.

Pope, S. A., Balikhin, M. A., Zhang, T. L., Fedorov, A. O., Gedalin, M., & Barabash, S. (2009). Giant vortices lead to ion escape from Venus and re-distribution of plasma in the ionosphere. *Geophysical Research Letters*, *36*, L07202. https://doi.org/10.1029/2008GL036977

Pu, Z. Y., & Kivelson, M. G. (1983). Kelvin-Helmholtz instability at the magnetopause. I—Solution for compressible plasmas. *Journal of Geophysical Research*, *88*, 841–852.

Ruhunusiri, S., Halekas, J. S., McFadden, J. P., Connerney, J. E. P., Espley, J. R., Harada, Y., … Hasegawa, H. (2016). Maven observations of partially developed Kelvin-Helmholtz vortices at Mars. *Geophysical Research Letters*, *43*, 4763–4773. https://doi.org/10.1002/2016GL068926

Sundberg, T., Boardsen, S. A., Slavin, J. A., Anderson, B. J., Korth, H., & Zurbuchen, T. H. (2012). MESSENGER orbital observations of large-amplitude Kelvin-Helmholtz waves at Mercury's magnetopause. *Journal of Geophysical Research*, *117*, A04216. https://doi.org/10.1029/2011JA017268

Taylor, M. G. G. T., Hasegawa, H., Lavraud, B., Phan, T., Escoubet, C. P., Dunlop, M. W., … Wild, J. A. (2012). Spatial distribution of rolled up Kelvin-Helmholtz vortices at Earth's dayside and flank magnetopause. *Annales Geophysicae*, *30*, 1025–1035. https://doi.org/10.5194/angeo-30-1025-2012

Thomas, V. A., & Winske, D. (1993). Kinetic simulations of the Kelvin-Helmholtz instability at the magnetopause. *Journal of Geophysical Research*, *98*, 11,425–11,438.

Walsh, A. P., Haaland, S., Forsyth, C., Keesee, A. M., Kissinger, J., Li, K., … Taylor, M. G. G. T. (2014). Dawn-dusk asymmetries in the coupled solar wind-magnetosphere-ionosphere system: A review. *Annales Geophysicae*, *32*, 705–737. https://doi.org/10.5194/angeo-32-705-2014

Walsh, B. M., Sibeck, D. G., Wang, Y., & Fairfield, D. H. (2012). Dawn-dusk asymmetries in the Earth's magnetosheath. *Journal of Geophysical Research*, *117*, A12211. https://doi.org/10.1029/2012JA018240

Walsh, B. M., Thomas, E. G., Hwang, K.-J., Baker, J. B. H., Ruohoniemi, J. M., & Bonnell, J. W. (2015). Dense plasma and Kelvin-Helmholtz waves at Earth's dayside magnetopause. *Journal of Geophysical Research: Space Physics*, *120*, 5560–5573. https://doi.org/10.1002/2015JA021014

Wang, C.-P., Gkioulidou, M., Lyons, L. R., & Angelopoulos, V. (2012). Spatial distributions of the ion to electron temperature ratio in the magnetosheath and plasma sheet. *Journal of Geophysical Research*, *117*, A08215. https://doi.org/10.1029/2012JA017658

Wing, S., Johnson, J. R., Newell, P. T., & Meng, C.-I. (2005). Dawn-dusk asymmetries, ion spectra, and sources in the northward interplanetary magnetic field plasma sheet. *Journal of Geophysical Research*, *110*, A08205. https://doi.org/10.1029/2005JA011086

Yan, G. Q., Mozer, F. S., Shen, C., Chen, T., Parks, G. K., Cai, C. L., & McFadden, J. P. (2014). Kelvin-Helmholtz vortices observed by THEMIS at the duskside of the magnetopause under southward interplanetary magnetic field. *Geophysical Research Letters*, *41*, 4427–4434. https://doi.org/10.1002/2014GL060589